Dual-Function Catalysis in Propane Dehydrogenation over Pt_1–Ga_2O_3 Catalyst: Insights from a Microkinetic Analysis

Qing-Yu Chang,† Kai-Qi Wang,† Ping Hu,† Zhi-Jun Sui,† Xing-Gui Zhou,† De Chen,‡ Wei-Kang Yuan,† Yi-An Zhu,†*

†United Chemical Reaction Engineering Research Institute (UNILAB), State Key Laboratory of Chemical Engineering, School of Chemical Engineering, East China University of Science and Technology, Shanghai 200237, China

‡Department of Chemical Engineering, Norwegian University of Science and Technology, N-7491 Trondheim, Norway

Abstract

The kinetics of propane dehydrogenation over single-Pt-atom-doped Ga_2O_3 catalyst has been examined by combining density functional theory calculations and microkinetic analysis. The doping of Pt not only can improve the selectivity of the Ga_2O_3 catalyst by hindering the deep dehydrogenation reactions but also helps to achieve a long-term stability by improving the resistance of Ga_2O_3 to hydrogen reduction. Microkinetic analysis indicates that upon Pt doping the turnover frequency for propane consumption is increased by a factor of 2.8 under typical operating conditions, as compared to the data on the pristine Ga_2O_3 surface. The calculated results suggest that the Pt_1-Ga_2O_3 catalyst shows a bifunctional character in this reaction where the Pt-O site brings about dehydrogenation while the Ga-O site is active for desorbing H_2, which provides a beautiful explanation for the previous experimental observation that even trace amounts of Pt can dramatically improve the catalytic performance of Ga_2O_3.

Keywords: Propane dehydrogenation; Single-site catalysis; Pt_1–Ga_2O_3; DFT; Microkinetic modeling

* Corresponding author: yanzhu@ecust.edu.cn (Yi-An Zhu)

INTRODUCTION

Light alkenes, which have traditionally been obtained from steam cracking and fluid catalytic cracking of naphtha, light diesel, and other oil products, are important feedstocks in the chemical industry for the production of polymers, oxygenates, and other important chemical intermediates.[1] The recent shale gas revolution, however, has promoted the production of low-cost light alkanes and therefore provided an attractive olefin production technology through dehydrogenation.[2] Propane dehydrogenation (PDH) has long been successfully commercialized, where Al_2O_3–supported PtSn and CrO_x catalysts are used due to their high propylene selectivity and stability.[3] On the other hand, much industrial chemical research has being devoted to the search for new and more effective catalysts because Pt is rather costly and hexavalent Cr is environmentally unfriendly. Hence, many oxides such as Ga_2O_3,[4-6] VO_x,[7-9] ZrO_2,[10-12] CeO_2,[13,14] ZnO,[15] TiO_2,[16] and Al_2O_3[17] have been extensively studied for PDH, among which Ga_2O_3 is a very promising candidate.

Recently, Sattler et al.[18] synthesized a 1000 ppm Pt–promoted 3 wt % Ga_2O_3/Al_2O_3 catalyst, which shows a high catalytic activity and stability in PDH. Interestingly, the conversion of propane (42.0 %) at 620℃ and 1 atm is almost twice the conversion when Pt is absent. In addition, the well-dispersed Pt–Ga_2O_3/Al_2O_3 catalyst is highly resistant to coke formation and remains active for long-term dehydrogenation-regeneration cycles. It is therefore of great interest to see why this minute amount of Pt can dramatically improve the catalytic performance of the Ga_2O_3 catalyst and to understand the important role that Pt and Ga_2O_3 have played in the dehydrogenation reaction. In that work, the authors postulated that the coordinatively unsaturated Ga^{3+} species are the active species for breaking C–H bond while Pt would assist in desorbing H_2, making the active sites available for the dehydrogenation cycle. More recently, similar catalysts were prepared by Im and Choi.[19] The only difference is that Pt was introduced during the synthesis of Ga_2O_3–Al_2O_3 through the sol-gel method and Ga_2O_3–Al_2O_3 was doped by atomically dispersed Ce, both of which may enhance the interaction between Pt and the substrate and avoid Pt sintering. The catalyst showed remarkably good catalytic performance and GaO_x was believed to be the main active site while Pt functions only as promoters.

Theoretically, Liu and co-workers studied PDH over the perfect Ga_2O_3(100)-A surface,[20] who proposed that the coordinatively unsaturated O sites are active for cleaving the C–H bonds in propane and are where propylene formed. However, the H atoms are bound too tightly to the O sites to desorb from the surface and may form water by reacting with these reactive O sites following the Mars van Krevelen mechanism. The Ga sites can then serve as the active sites for dehydrogenation reactions once the surface O ions are removed.[20] Hence, despite the many studies, it remains elusive how the trace amount of Pt can dramatically promote PDH over the Ga_2O_3 catalyst and there is still no direct evidence that may support the speculations about how the Pt and Ga_2O_3 actually work.

Actually, despite the superior catalytic performance of single-atom catalysts (SACs) in many reactions of commercial importance,[13,21-32] the nature of the active phase is not always clear, which is due primarily to the increased complexity in the electronic structure that arises from the change in surface composition.[33] For instance, it has been demonstrated that coadsorption of a pair of amphoteric species (e.g., propyl and H in PDH) could be significantly more stable than the adsorption of the isolated species on many oxide surfaces due to Lewis acid-base interaction,[34-36] which makes it possible to tailor the catalytic properties of oxides to a particular chemical reaction by doping the surfaces with single metal atoms. In this way, either single metal atoms or their immediate surroundings could make a major contribution to the kinetics of the reaction,[37,38] and sometimes they could even function cooperatively, showing a bifunctional character.[39]

Understanding the nature of active sites for a specific reaction is of crucial importance, especially in the field of single-site heterogeneous catalysis where a high degree of site heterogeneity often exists. In this work, by combining DFT calculations and microkinetic analysis, the kinetics of PDH on pristine and single Pt atom–doped Ga_2O_3(100) is studied to explain the key role of atomically dispersed Pt on the enhanced catalytic performance of the Ga_2O_3 catalyst. The geometrical and electronic structures of the two surfaces are first analyzed. Then, energy decomposition and Bader charge analysis are conducted to quantitatively measure the strength of Lewis acid-base interaction and its effect on the adsorption behavior of the surfaces. Next, the elementary steps involved in the network of the main and side reactions, together with the migration of H on the oxide surfaces are investigated. After that, microkinetic analysis is performed to identify the active site and rate-limiting step. Finally, we conclude by discussing the implication of our results for the explanation of the bifunctional character of the Pt_1–Ga_2O_3 catalyst.

COMPUTATIONAL DETAILS

DFT calculation

Spin-polarized DFT calculations were performed using the Vienna ab initial Simulation Package (VASP).[40-42] The generalized gradient approximation (GGA) with the Bayesian error estimation functional with van der Waals correlation (BEEF-vdW)[43] was used to treat the exchange and correlation of the Kohn-Sham theory. The interactions between ion cores and valence electrons were represented by the projector-augmented wave (PAW) method. Because the "hard" PAW potentials with electron configurations of H ($1s^1$), C ($2s^2$ $2p^2$), O_s ($2s^2$ $2p^4$), Ga_d ($3d^{10}$ $4s^2$ $4p^1$), and Pt ($5d^9$ $6s^1$) were used, an energy cutoff of up to 600 eV was found to be essential for the convergence of the total energy per atom to within 1 meV. The Gaussian smearing method with an energy smearing of 0.1 eV was used to determine the partial occupancies of the orbitals. Geometry optimization was considered to be converged when the forces on each atom were less than 0.03 eV/Å. The transition states were located by either the dimer method[44] or the climbing-image nudged elastic band (CI-NEB)

method,[45,46] which have been verified to have only one imaginary frequency by vibrational frequency analysis. The adsorption energy of species (ΔE_{ads}) was calculated as

$$\Delta E_{ads} = E_{surface+adsorbate} - E_{surface} - E_{adsorbate} \quad (1)$$

where $E_{surface+adsorbate}$, $E_{surface}$, and $E_{adsorbate}$ are the total energies of surface with adsorbate, surface, and gas-phase adsorbate, respectively.

Structural model

The bulk structure of β-Ga_2O_3 was optimized using the quasi-Newton algorithm, during which both the lattice vectors and atomic coordinates were relaxed. The results were converged when the forces on each atom were less than 0.01 eV/Å. The optimized cell parameters of β-Ga_2O_3 are a = 12.46 Å, b = 3.09 Å, c = 5.89 Å, and β = 103.71°, which agree well with the experimental[47,48] and other theoretical values[49-51]. The energetically most favorable and most widely studied Ga_2O_3(100)-B termination[49,52-54] is taken into account in this work. The Ga_2O_3(100) slab model with a $p(3 \times 2)$ supercell was then cleaved, consisting of 120 atoms in two unit layers, as shown schematically in Figure 1. The bottom two layers were fixed, while the top four layers and the adsorbed species were allowed to relax during the calculations. A vacuum layer as thick as 12 Å was inserted between adjacent slabs along the z axis. A Γ-centered 3 × 3 × 1 Monkhorst-Pack k-point grid was used to sample the first Brillouin zone of the system.

Since single metal atoms may be adsorbed on the pristine oxide surface,[33] located in the cation vacancy,[55] or even in the oxygen vacancy,[56,57] calculations have been performed on various configurations to construct a reasonably accurate description of atomic Pt atoms dispersed on Ga_2O_3(100). As shown in Figure S1, adsorption of a single Pt atom onto the pristine surface is less stable than that onto the defective surfaces. In particular, substitution of Pt for Ga(o) (o stands for octahedral) is thermodynamically most favorable with a binding energy of −9.65 eV, thereby providing a rational interpretation of the experimentally observed increase in the proportion of the tetrahedrally coordinated Ga^{3+} species upon doping the Ga_2O_3 surface with Pt.[18] Furthermore, the binding energy is much more negative than the calculated cohesive energy of bulk Pt at the same level of theory (−5.08 eV), indicating that the Pt–substrate interaction is sufficiently strong to inhibit Pt clustering,[58] in accord with the experimental observation that the interaction between Pt and Ga_2O_3 is so strong that the mobile Pt could be captured by Ga_2O_3.[59] For this reason, the Pt_1–Ga_2O_3(100) slab model shown in Figure 1 was finally adopted.

Microkinetic analysis

Microkinetic analysis was carried out based on a mean-field model and the kinetic model was solved by using the CatMAP code[60] under typical PDH experimental conditions at 895 K and 1 bar of C_3H_8.[18] Corrections to the entropy and

enthalpy of gas-phase molecules and adsorbed species were made under the ideal-gas approximation and harmonic approximation, respectively. The rate constant (k) for elementary steps was evaluated according to the following equation within the framework of the transition state theory (TST)[61]:

$$k = \frac{k_B T}{h} e^{\Delta S^{o\ddagger}/k_B} e^{-\Delta H^{o\ddagger}/k_B T} \quad (2)$$

where k_B, h, $\Delta S^{o\ddagger}$, $\Delta H^{o\ddagger}$, and T are Boltzmann's constant, Planck's constant, the entropy change from the initial to the transition state, the enthalpy change from the initial to the transition state, and temperature, respectively.

The reaction rates (r_i) were obtained by solving the mean-field microkinetic model to steady state. The differential equations are:

$$r_i = k_i^+ \prod_n \theta_{in} \prod_n p_{in} - k_i^- \prod_l \theta_{il} \prod_l p_{il} \quad (3)$$

$$\partial \theta_j / \partial t = \sum_i s_{ji} r_i \quad (4)$$

where $k_i^{\pm}$, $\theta_{in/il}$, $p_{in/il}$, and s_{ji} are the forward/reverse rate constant, the surface concentration of the adsorbed reactants/products for elementary step i, the unitless pressure of the gas-phase reactants/products for elementary step i, and the stoichiometric coefficient of species j in elementary step i, respectively. This set of coupled non-linear ordinary differential equations has a steady-state solution as

$$\partial \theta_j / \partial t = 0 \quad (5)$$

which is solved subject to the site conservation constraint:

$$\sum_j \theta_j = \theta^{TOT} \quad (6)$$

where θ^{TOT} is the normalized surface area.

The degrees of rate control were calculated to identify the rate-determining transition states and intermediates on the basis of the Campbell's method[62,63] as implemented in the CatMAP code. The definition of degree of rate control is:

$$X_{ij} = \frac{d\, log\left(r_i\right)}{d\left(-G_j / k_B T\right)} \quad (7)$$

where X_{ij}, r_i, G_j, k_B, and T are the degree of rate control matrix, the production rate for product i, the free energy of species j, Boltzmann's constant, and temperature, respectively.[60]

RESULTS AND DISCUSSION

Geometrical and electronic structures of Pt_1–Ga_2O_3(100)

Metal-oxide surfaces usually have a high degree of site heterogeneity,[17] which provides an opportunity for understanding site-dependent catalysis and designing optimal catalysts under the guidance of structure-activity relationships.[64] On the outermost layer of the pristine Ga_2O_3(100) surface, there exist three distinct types of ions, namely, octahedrally coordinated Ga(o), tetrahedrally coordinated Ga(t), and threefold coordinated O, as shown in Figure 1a. Ga(o) and O ions are coordinatively unsaturated compared to their counterparts in the bulk and may therefore show reactivity. Upon doping Ga_2O_3(100) with Pt atoms, apart from the Pt site, two Ga(o)′ sites and four O′ sites are newly formed surrounding each single Pt atom, as shown in Figure 1.

Charge density difference upon adsorption of Ga(o)/Pt in the metal vacancy is first analyzed to study the charge redistribution in the oxide lattice. As shown in Figure 1b and 1c, the charge redistribution is localized around the Ga(o)/Pt cation and its five nearest neighbor oxygen anions, in accord with the fact that the Ga ions in the "irreducible" Ga_2O_3 can hardly accommodate extra electrons. Previously, it has been demonstrated that the opposite is true of "reducible" oxides such as CeO_2, on which charge transfer may readily take place between doped single metal ions and the surrounding Ce ions.[58]

The localized charge redistribution can further be confirmed by performing the Bader charge analysis. It can be seen in Table S1 that upon adsorption the charges carried by the ions other than the Ga(o)/Pt and its five nearest neighbor oxygen ions remain almost constant. The single Pt atom becomes positively charged and loses 1.19 electrons upon adsorption in the vacancy. By comparison, 1.85 electrons are transferred from the Ga(o) ion to the nearest neighbors. As a result, the surrounding O′ and O ions on the topmost layer accept 1.13 and 1.26 electrons, respectively. The single Pt atom behaves like a low-valence dopant in this sense,[65] and the reactivity of its neighboring O′ ions may be considerably enhanced compared to those coordinated to the Ga(o) ions.

To examine more closely the modification of the electronic structure of Ga_2O_3(100) upon Pt doping, the density of states (DOS) projected onto the metal valence shell and the O 2*p* orbital are then calculated. One can see from Figure 1d that, at the Ga–O site, there are occupied O 2*p* orbitals near the Fermi level but neither obvious occupied nor unoccupied Ga 4*s*/4*p* orbitals are found in the vicinity and the Ga 3*d* orbitals are mainly present in the region below −12 eV, indicating the O 2*p* orbitals would play a dominant role in determining the strength of the adsorbate-substrate interaction.

At the Pt–O′ site, the Pt 5*d* and O′ 2*p* orbitals are strongly hybridized in the region from −8 eV to the Fermi level (see Figure 1e), which may account for the high stability of Pt substitution in the Ga(o) vacancy.[66] The peaks of the Pt 5*d* orbitals appear on both sides of the Fermi level, indicating both the occupied and unoccupied frontier 5*d* orbitals of Pt can interact with adsorbed species. Hence, a highly reactive single Pt atom could be expected. The orbitals of the Ga(o)′ ion

resemble that of the Ga(o) ion on the pristine surface, implying that the introduction of single Pt atom may have a minor influence on the electronic structure of the Ga(o)′ ions nearby.

Adsorption property of Pt_1–Ga_2O_3(100)

As has previously been suggested,[34] Lewis acid-base interaction often influences the adsorption properties of metal oxides, in which adsorption of a Lewis acid at the metal site may be enhanced by the coadsorption of a Lewis base at an adjacent O site. We also found recently that this interaction occurs only on "irreducible" metal oxides.[67] Here the "reducibility" of oxides refers to the ability of the metal cation to accommodate extra electrons that are donated by Lewis bases upon their adsorption at the adjacent O site, which requires that the metals be able to exist in a lower oxidation state other than zero. As Ga has only one stable oxidation state of +3 in forming metal oxides, the Lewis acid-base interaction is expected to occur on the "irreducible" Ga_2O_3. As for Pt_1–Ga_2O_3(100), however, the situation becomes much more complicated. The Pt itself may exhibit various oxidation states. When embedded in the oxide lattice of Ga_2O_3, as aforementioned, it has an effect on the electronic structure of the surroundings. Hence, of particular interest is how the electron transfer between Pt, Ga, O, and adsorbates would affect the strength of the Lewis acid-base interaction, and hence the adsorption behavior of the metal-oxide surface.

The optimized geometries of reactants, products, and intermediates adsorbed on Pt_1–Ga_2O_3(100) are shown in Figure S2 and the calculated adsorption energies are summarized in Table 1. It is clear that propane and H_2 are weakly physisorbed on the surface without bond formation. Furthermore, the calculated adsorption energies fall within the typical ranges of the physisorption energies of propane and H_2 (−0.2 ~ –0.4 eV and –0.05 ~ –0.2 eV for propane and H_2, respectively), as has been observed on metal surfaces[68-70] and other oxide surfaces[12,17].

Both physisorption and chemisorption of propylene have been taken into consideration. The physisorption energies of propylene are −0.35 eV, implying that propylene physisorption is a moderately exothermic process. By analogy to our previous findings on the Cr_2O_3 and ZnO surfaces,[67] the chemisorption energies of propylene are positive at the Ga(o)–O and Ga(o)′–O′ sites but become negative when it forms bond to surface Pt ions. At the Pt–O′ site and on top of the Pt ion, propylene is chemisorbed in the di-σ and π modes, respectively, releasing 0.36 and 0.59 eV of heat.

To figure out why physisorption of propylene is preferred at some sites but formation of covalent bonds is energetically more favorable at others, the adsorption energies of propylene are divided into three terms:

$$\Delta E_{ads} = \Delta E_{distortion,surf} + \Delta E_{distortion,ads} + \Delta E_{bonding} \quad (8)$$

where $\Delta E_{distortion,surf}$ and $\Delta E_{distortion,ads}$ are the distortion energies of the surface and propylene upon adsorption, respectively, and $\Delta E_{bonding}$ is the bonding energy that measures the strength of the direct interaction between distorted

propylene and surface. As can be seen in Figure 2, when propylene is physisorbed on the surface, the $\Delta E_{distortion,surf}$ and $\Delta E_{distortion,ads}$ are negligibly small and, consequently, the ΔE_{ads} is determined largely by the $\Delta E_{bonding}$. Upon chemisorption, the $\Delta E_{distortion,surf}$ and $\Delta E_{distortion,ads}$ are highly positive at the Ga(o)–O and Ga(o)′–O′ sites, indicating the surface and propylene are significantly distorted, which have a negative effect on the attachment. Thus, the adsorption processes at the two sites are endothermic, though the $\Delta E_{bonding}$ is as negative as −3.77 and −3.33 eV. When propylene forms bond with Pt, the distortion energies, although still positive, become much less positive at the Pt–O′ site and even close to zero at the Pt atop site. It is interesting to find that, although the $\Delta E_{bonding}$ at the Pt–O′ site is comparable to those at the Ga(o)–O and Ga(o)′–O′ sites, the smaller distortion energy causes the adsorption process to show an exothermic character. By comparison, the bonding at the Pt atop site is actually quite weak, but the overall chemisorption process is exothermic because the energy released by the formation of bonds more than offsets the small amount of energy that must be expended to overcome the local geometrical distortions.

At the Ga(o)–O site, the reaction intermediates, including H, 1-propyl, and 2-propyl, are preferentially coordinated solely to the O ion, in accord with the aforementioned DOS analysis that the O site would play a major role in the adsorbate–surface interaction. At the Ga(o) site, the H atom is only weakly chemisorbed, and 1-propyl and 2-propyl even cannot form covalent bonds to the surface, indicating the Ga(o) ions show rather low reactivity. When the intermediates are positioned at the Ga(t) site, they would be relaxed to the adjacent O site upon geometry optimization, which is due to the saturated coordination environment of the Ga(t) ion.

If we move to O′ site that is bonded to Pt, the adsorption energies of the species become more negative than those at the O site. The reason for this observation is that fewer electrons are gained by the O′ ion from the adjacent Pt ion than by the O ion from Ga(o), which can only be compensated for by the electron density shift from the adsorbate towards the O′ ion, leading to a stronger electrostatic attraction between the positively charged adsorbate and the negatively charged O′ ion. From Table 1, it can be seen that the energy changes for H adsorption at the Ga(o) and Ga(o)′ sites are −0.16 and −0.37 eV, respectively, during which 0.20 and 0.26 electrons are transferred from the surface to the H adsorbed, meaning that the surface around the Ga(o)′ ion is more capable of donating electrons to the adsorbate with the introduction of Pt. It is important to note that the Ga(o)′ ion also gains electrons from its nearest neighbor O′ ions, which is facilitated by the electron donation by the doped Pt.

Although both the O′ and Ga′ ions become more reactive upon Pt doping, the Pt ion itself is thermodynamically most favorable for chemisorption of the reaction intermediates. Interestingly, when the adsorbates are coordinated to the Pt ion,

the flow of electron density is in the opposite direction to that at the Ga(o)/Ga(o)′ sites and the majority of the electrons donated by H are accepted by Pt. In this regard, the Pt behaves completely differently from it does when H is attached to the Ga(o)′ site, and its ability to either gain or lose electrons can be attributed to the aforementioned coexistence of the occupied and unoccupied frontier 5*d* orbitals near the Fermi level.

Lewis acid-base interaction

From the data given above, it is clear that on the metal-oxide surfaces charge transfer is particularly important in studies of their adsorption and catalytic properties. The question that now arises is whether there exists a qualitative relationship between the electron transfer and adsorbate-substrate interaction and how this relationship, if any, can be expressed in terms of energetic and electronic properties. Actually, it has already been demonstrated that the Lewis acid-base interaction occurs when a pair of amphoteric species is coadsorbed at the M–O site on "irreducible" oxide surfaces, which would significantly enhance the bonding between the adsorbates and the surfaces.[34,67] However, the strength of this interaction has not yet been quantitatively measured.

Intuitively, one may define the Lewis acid-base interaction as the difference between the coadsorption energy of a pair of amphoteric species and the sum of the adsorption energies when they are individually adsorbed (i.e., $\Delta E_{coads} - \Delta E_{ads,acid} - \Delta E_{ads,base}$). The more negative the value, the greater is the interaction. However, the Lewis acid-base interaction is essentially an electronic effect that arises purely from electron transfer. Any contributions from surface and adsorbate distortion should be differentiated from the ligand effect and removed from the energy difference given above. A straightforward way is to express the Lewis acid-base interaction ($\Delta E_{int,acid-base}$) as a difference in the bonding energy between coadsorption and individual adsorption:

$$\Delta E_{int,acid-base} = \Delta E_{bonding,acid+base} - \Delta E^{constrained}_{bonding,acid} - \Delta E^{constrained}_{bonding,base} \quad (9)$$

where the $\Delta E_{bonding,acid+base}$, $\Delta E^{constrained}_{bonding,acid}$, and $\Delta E^{constrained}_{bonding,base}$ are calculated with the geometries of the distorted adsorbates and surface constrained to those upon coadsorption. Substitution into and rearrangement of eq 9 gives

$$\Delta E_{int,acid-base} = E_{surf+acid+base} + E^{constrained}_{surf} - E^{constrained}_{surf+acid} - E^{constrained}_{surf+base} \quad (10)$$

where $E_{surf+acid+base}$, $E^{constrained}_{surf}$, $E^{constrained}_{surf+acid}$, and $E^{constrained}_{surf+base}$ are the total energies of the oxide surface with the acid and base coadsorbed, the constrained surface, the coadsorption configuration with the base removed, and the coadsorption configuration with the acid removed, respectively. The details of the derivation of these equations are included in the Supporting Information. Under this definition, a more negative $\Delta E_{int,acid-base}$ indicates a stronger Lewis acid-base interaction.

The calculated $\Delta E_{int,acid-base}$ values for the coadsorbed reaction intermediates in PDH are summarized in Table 2. One can see from the table that the $\Delta E_{int,acid-base}$ at the Ga(o)–O and Ga(o)′–O′ sites are highly negative (more negative than −1 eV). In contrast, the value is slightly positive at the Pt–O′ site, meaning that the Lewis acid-base does not occur. Furthermore, the $\Delta E_{int,acid-base}$ at the Ga(o)′–O′ sites is less negative than that at the Ga(o)–O site, indicating that the Lewis acid-base interaction becomes weaker around the Ga(o)′ and O′ ion pair upon Pt doping.

By comparing the $\Delta E_{int,acid-base}$ with the $\Delta E_{coads} - \Delta E_{ads,acid} - \Delta E_{ads,base}$, we can see that in general the former is more negative or less positive, which is due to the fact that the surface and adsorbate are distorted more dramatically upon coadsorption. The only exception occurs at the Ga(o)–O site. When a single H atom is adsorbed at the Ga(o) site, the adsorbate-substrate interaction is so weak that the Ga(o) cation protrudes from the oxide surface to minimize its coordination number, thereby enhancing the bonding but giving rise to a great surface deformation. Upon coadsorption, the H atom at the Ga(o) site is stabilized by the Lewis acid-base interaction, and, consequently, the surface is much less distorted.

Since the Lewis acid-base interaction results essentially from the electron transfer accompanying coadsorption, it is good practice to carry out electronic structure analysis to visualize how the adsorbate and surface behave during the process and to confirm the predictions made by the calculations of energetic properties. Thus, the charge density difference for H adsorption at the O site with another H atom pre-adsorbed at the Ga(o), Ga(o)′, and Pt site is computed and illustrated in Figure 3. It can be seen that at the Ga(o)–O and Ga(o)′–O′ sites there is clearly a flow of electrons between the two coadsorbed H through the surface. Comparison between the calculated effective Bader charges (see Tables 1 and 2) confirms that 0.16 and 0.11 electrons are gained by the negatively charged H at the Ga(o)–O and Ga(o)′–O′ sites, respectively. In essence, the electrons donated by the positively charged H are to increase the electron density around the Ga and O ion pair, which in turn enhances the ability of the Ga ion to donate electrons to the H thereon, making bond formation energetically more favorable.

At the Pt–O′ site, however, the vast majority of the electrons donated by the H at the O′ site are gained by the O′ and Pt ions. Under such a circumstance, the electron-deficient Pt ion may exist in a lower stable oxidation state and therefore transfers only 0.06 electrons to the negatively charged H. As a result, the Lewis acid-base interaction does not occur, consistent with the quantitative predictions by the $\Delta E_{int,acid-base}$.

PDH on Pt_1–Ga_2O_3(100)

It follows from the stoichiometry of the PDH reaction that the reaction scheme involves two successive dehydrogenation steps followed by desorption of propylene and H_2 from the catalyst surface. However, although the net reaction is very simple, the mechanism by which it occurs is rather complex and has not yet been fully elucidated, especially for metal-oxide catalysts. The reason is probably due to the fact that, apart from the dehydrogenation and desorption steps, many side reactions such as the deep dehydrogenation, C–C bond cleavage, H migration, and H_2O formation need to be taken into consideration.

The first dehydrogenation step

It is well known that the C–H bond in alkanes can be activated by the M–O and O–O/M–M pairs on oxide surfaces via the heterolytic and homolytic mechanisms, respectively. Kazansky et al. proposed that ethane would be dissociated heterolytically on gallium-oxide surfaces, giving rise to C_2H_5–Ga and H–O,[71] and the formation of gallium–alkyl species upon interaction of small alkanes with gallium oxide has been verified experimentally by solid-state NMR.[72] Thus, the C–H bond is more likely to be activated at the M and O ion pair.

The energy profiles for the main reaction of PDH, together with the geometries of the transition states for the elementary steps involved, are shown in Figure 4, where the lengths of the activated C–H bonds are also given. From the figure, one can see that the energy barriers for the formation of 1-propyl&H and 2-propyl&H at the Ga(o)–O site are 1.64 eV and 1.48 eV, respectively, indicating the C–H bond in the methylene group is more readily activated than that in the methyl group. As discussed in Sec. 3.3, the energies of the final states are determined largely by the Lewis acid-base interaction that arises from the electron transfer from the Lewis base to the acid. To examine if the Lewis acid-base interaction plays a role in determining the energy of the transition states, Bader's analysis was also carried out on the TS3. It is found that the charges on the 2-propyl and H are 0.30− |e| and 0.41+ |e|, respectively. Compared with their counterparts in the final state, the 2-propyl carries the same number of electrons while the H becomes less positively charged by 0.13 |e|. The reason for the lowering of the electron density shift away from the H is due to the fact that, although the transition state closely resembles the final state, the H that is coordinated solely to the O ion in the final state forms an additional bond with the Ga(o) ion (see Figure 4 and Figure S2). Nevertheless, the negatively and positively charged coadsorbed species clearly indicate that the Lewis acid-base interaction persists in the transition state. Moreover, considering that the $\Delta E_{int,acid-base}$ is as negative as −1.33 eV for the coadsorbed 2-propyl and H, the activated complex must have been substantially stabilized by the presence of the interaction, which makes the reaction kinetically feasible at the typical PDH reaction temperatures.

Upon doping the oxide surface with a single Pt atom, either the Ga(o)′–O′ or Pt–O′ site could be active for the cleavage of the C–H bond in propane. From Figure 4, it can be seen that compared with the dehydrogenation barriers at the Ga(o)–O site, the activation energies for the formation of 1-propyl&H and 2-propyl&H are increased by 0.20 and 0.24 eV,

respectively, at the Ga(o)′–O′ site and lowered by 0.23 and 0.24 eV, respectively, at the Pt–O′ site. At the Ga(o)′–O′ site where the Lewis acid-base interaction takes place, the $\Delta E_{int,acid-base}$ for the coadsorbed 2-propyl and H is reduced by 0.24 eV going from the Ga(o)–O site to the Ga(o)′–O′ site, which leads to a rise in the energy of the final states. According to the BEP relationship which states that there is a linear relationship between the activation energy of an elementary step and the heat of reaction if entropy effects are neglected,[73] it is reasonable to expect that the activated complexes are less stabilized at the Ga(o)′–O′ site, which helps explain the observed increase in the activation energy. On the other hand, as suggested in Sec. 3.2 and Sec. 3.3, the Pt ion is thermodynamically very favorable for chemisorption of the reaction intermediates and the reactivity of the O′ ion is enhanced by Pt doping. Thus, it is not surprising to learn that the transition state energies are more negative at the Pt–O′ site than at the Ga(o)–O site.

H surface diffusion

After one H atom is abstracted from the propane molecule, it would be adsorbed at the O/O′ site adjacent to the Ga-propyl or Pt-propyl species. In the mean-field approximation, the adsorbed species are distributed randomly over the surface and there is no interaction between the adsorbates. Hence, in the previous studies over transition-metal catalysts,[68,69,74] the adsorbed propyl and H are thought of as widely separated species and H has no effect on the kinetics of the subsequent dehydrogenation reactions. However, as we know, the mean-field approximation tends to be valid when the adsorbates repel one another and when the surface coverage is low. For attractive interactions, as is the case for the coadsorbed propyl and H at the Ga–O sites, this approximation often breaks down and, consequently, the coupling between transport and reaction becomes essential to an accurate description of the reaction kinetics. On the other hand, it is generally accepted that high reaction temperatures such as that applied in PDH tend to randomize the adsorbed species across the surface. As a consequence, the attractive interactions between the coadsorbed species might be overcome and the adsorbates may move freely about the surface. Thus, to explore whether the adsorbate-adsorbate interaction would affect the overall reaction rate, H diffusion is examined in the presence and absence of 2-propyl around both the Ga(o)–O and Pt–O′ sites, where coadsorption of 2-propyl and H and individually adsorbed H are taken as the initial states for the migration process, respectively.

Considering the site heterogeneity on the oxide surfaces, there exist three possible elementary steps for H migration between adjacent O sites on the surfaces around the Ga(o) and Pt ions, regardless of whether or not 2-propyl is adsorbed in the vicinity, as illustrated in Figure 5a–d. Here the H hopping between O and Ga is disregarded because the difference in the H adsorption energy between the two sites would give rise to a migration barrier of more than 2 eV, making the process kinetically hindered. The calculated migration barriers for all the elementary steps are summarized in Figure 5e, which indicate that H migrates invariably preferentially along the [010] axis on Pt_1–Ga_2O_3(100). Although the H migration barrier

for the kinetically most favorable step varies from case to case, all of them fall in the range of 0.7 – 1.4 eV, which can be readily surmounted at typical PDH operating temperatures. Therefore, the mean-field approximation does hold over the oxide surfaces and can be invoked to reveal the kinetics of the PDH reaction.

Interestingly, by comparing the energy barriers for steps *a* and *a″* as well as those for steps *a′* and *a‴*, we find that the presence of 2-propyl at the metal site would accelerate H diffusion along the kinetically most favorable path, even if the interaction between the coadsorbed species is attractive at the Ga(o)–O site. To provide a physical interpretation for this phenomenon, the adsorption energy of H with 2-propyl coadsorbed on the surface is decomposed for both the initial and the transition states by analogy to eq 8:

$$\Delta E_{ads,H} = \Delta E_{distortion,surf+2-propyl} + \Delta E_{distortion,H} + \Delta E_{bonding,H}^{constrained} + \Delta E_{int,2-propyl-H} \quad (11)$$

In this way, the interaction energy between 2-propyl and H can be connected with the adsorption energy of the hopping H, and hence with the migration barrier. The details of the derivation of the equation and the values of the energy components are given in the Supporting Information (Sec. 7 and Table S2). It is found that the $\Delta E_{int,2-propyl-H}$ becomes less negative from −1.33 eV to −0.41 eV when H migrates along step *a*, which signifies that indeed the Lewis acid-base interaction contributes to increase the energy barrier. The reason that step *a* has a lower energy barrier than step *a″* is because a much more significant surface reconstruction takes place when H moves into the transition state in the absence of 2-propyl. At the Pt–O site, however, the repulsive interaction between 2-propyl and H is the major factor influencing the trend in the migration barrier.

The second dehydrogenation step

Since H is relatively free to move about the surface, it can be assumed that there is no coadsorbed H in the vicinity of propyl during the course of the second dehydrogenation step. In the TS2 and TS4 (see Figure 4a and 4b), the H atom is abstracted from physisorbed 1-propyl and 2-propyl by the O ion of the Ga(o)–O site, with energy barriers of 0.73 eV and 0.68 eV, respectively, much lower than those for the first dehydrogenation step.

Upon Pt doping, the second dehydrogenation step could occur around both the Pt and the Ga(o)′ ions. It can be seen from Figure 4a and 4b that the geometries of the transition state are distinctly different from those at the Ga(o)–O site and the radical mechanism no longer prevails. When the propyl fragments are activated at the Pt–O′ site, the carbon-containing species and H in the TS2′ and TS4′ are coordinated to the Pt and O′ ion, respectively. In the TS2″ and TS4″, the active site changes to the O′–Ga(o)′–O′ ensemble, where the propylene molecules are adsorbed at the Ga(o)′ and O′ ion pair with H abstracted by another O′ ion. Compared with the dehydrogenation barriers at the Ga(o)–O site, the activation energies for the 1-propyl and 2-propyl dehydrogenation are increased by 1.07 and 1.09 eV at the Pt–O′ site and by 1.08 and 1.13 eV at

the O′–Ga(o)′–O′ ensemble, respectively. The explanation is probably that the propyl fragments are strongly chemisorbed at the Pt and O′ sites (see Figure S2) but weakly physisorbed on top of Ga(o) ion and the more stable initial states at the Pt–O′ and Ga(o)′–O′ sites leads to the much higher energy barriers. Nevertheless, the overall energy profiles for the dehydrogenation of propane to propylene at the Pt–O′ site is relatively flat compared to those at the other two sites, indicating that the doped Pt is likely to dominate the C–H bond activation.

Apart from the active sites concerned, the oxygen vacancies and Ga(t) ions may have an effect on the catalytic behaviors of the Ga_2O_3-based catalysts[67,1]. Thus, the catalytic activities of these sites have been examined by removing a neutral oxygen atom from the outermost layer of Ga_2O_3(100) and by constructing a new surface termination that has Ga(t) exposed. The calculated potential energy diagrams for the main reaction of PDH are presented in Figures S3–S4 in the Supporting Information, which suggest that the Ga(o)–O site and oxygen vacancy show similar activities toward propane activation while the activity of Ga(t)-O is slightly lower. If we further consider the small number of the Ga(t) sites on the thermodynamically unstable corrugated surface, it is reasonable to expect that the Ga(t) site plays a minor role in determining the kinetics of PDH.

Hydrogen recombination and water formation

In an early study, Collins et al.[75] observed from infrared spectra that Ga–H and Ga–OH bonds can be simultaneously formed by the heterolytic cleavage of hydrogen on Ga/SiO_2, which was later confirmed by the experimental and theoretical results by Pan et al.[53] In light of this information, for the reverse of H_2 dissociation to take place, H atoms need to migrate to adjacent Ga(o) and O sites before they can recombine to desorb from the surface. However, as aforementioned, the H atoms that are abstracted from propane and propyl would be initially adsorbed at the O site and can hardly hop to the Ga(o) site due to a high energy barrier (> 2 eV).

Interestingly, the situation becomes completely different if two H atoms are coadsorbed at two O sites in the Ga(o)–O_4 ensemble. In this case, the lowest energy barrier for one of the H atoms to migrate from the O site to the Ga(o) site is calculated to be only 0.33 eV (see Figure S5), even lower than that for H hopping between O sites. In the transition state, the $\Delta E_{int,acid-base}$ takes a value of −0.56 eV, indicating the Lewis acid-base interaction has an enormous effect on the H surface transport behavior of the Ga_2O_3 catalyst. Thus, it can be deduced that the detached H will hop between the O sites along the [010] axis until it encounters another H atom in the same Ga(o)–O_4 ensemble, where coadsorption of two H atoms at the Ga(o) and O ion pair can be achieved. Upon Pt doping, although the energy barrier for H migration from O′ to Pt in the presence of a coadsorbed H is 0.27 eV higher than that at the Ga(o)–O site, the process is also kinetically feasible. The Pt–O′ site may accommodate a pair of H atoms unless it has already been occupied by reacting and resulting C3 species.

As illustrated in Figure 6, the coadsorbed H atoms may either recombine to form H_2 or react with surface O ion to produce water. The energy barriers for the formation of H_2 and H_2O at the Ga(o)–O site are predicted to be 0.53 and 1.94 eV, respectively, indicating that desorption of H_2 is kinetically preferred over the production of H_2O, in accord with the experimental observation that silica-supported Ga_2O_3 is difficult to be reduced by H_2 at 873K.[76] When Pt is doped on the surface, the energy barrier for the formation of H_2O is increased by 0.10 eV compared to that on the pristine surface, implying that the single Pt atom doping would further improve the resistance of Ga_2O_3 to hydrogen reduction and achieve a long-term stability of the catalyst. These findings agree well with the TPR experiment that no apparent H_2 consumption was detected even if the Pt–Ga_2O_3 catalyst has been heated up to 1073 K.[19] Besides, the energy barrier (1.28 eV) for the recombination of H atoms to produce H_2 is significantly higher than that at the Ga(o)–O site. Considering the very low abundance of single Pt atoms on the oxide surface, the Pt–O′ site cannot play a major role in hydrogen recombination.

Deep dehydrogenation of propylene

Deep dehydrogenation of propylene is directly related to the selectivity toward propylene, which can be measured by comparing the energy barriers for propylene dehydrogenation and desorption in the sense that the entropy of the activated complex in molecular desorption compares closely to that of the adsorbed species.[61,69] On the Pt catalyst, propylene would continue to be deeply dehydrogenated until propyne is formed, which was suggested to be the starting point for C–C bond breaking to give rise to the reaction by-products such as ethylene, methane, and coke.[68] Armed with this knowledge, we are now in a position to consider the side reactions over the Pt_1–Ga_2O_3 catalyst.

As shown in Figure 7a and 7b, the scission of the C–H bonds in propylene can occur in either the methylene or the methylidyne group, leading to the formation of 1-propenyl and 2-propenyl, respectively. One can see that the energy barriers for the deep dehydrogenation at the Ga(o)–O site (1.43 eV and 1.60 eV for the formation of 1-propenyl&H and 2-propenyl&H, respectively) are higher than the desorption activation energy (0.36 eV), suggesting that propylene can be readily released from the pristine surface, in accord with the experimental finding that the selectivity toward propylene over the β-Ga_2O_3 catalyst can be as high as 95% when the steady state is reached.[5] At the Pt–O′ and Ga(o)′–O′ sites, propylene desorption remains kinetically more favorable than deep dehydrogenation, but the activation energy difference becomes slightly smaller. On the other hand, the energy barriers for the subsequent 1-propenyl and 2-propenyl dehydrogenation reactions are increased dramatically by 1.79 and 1.61 eV, respectively, relative to those at the Ga(o)–O site whereas the activation energies for propenyl hydrogenation are lowered to 1.10 and 0.88 eV, which indicate that the propenyl groups tend hydrogenate to produce propylene rather than undergoing dehydrogenation to form propyne. Thus, the selectivity of the Ga_2O_3 catalyst toward propylene production can be improved by Pt doping, as has been evidenced by Sattler et al. who proposed a 96.9% selectivity of the well-dispersed Pt–Ga_2O_3/Al_2O_3 catalyst.[18]

C–C bond cleavage of C3 species

It was reported that the selectivity toward propylene can vary from 73% to 95% over GaO_x-based catalysts, depending on the loading of Ga_2O_3, choice of support, preparation method, and reaction conditions.[1] Hence, although the side reactions can be suppressed to a large extent, the cracking of C3 derivatives always occurs. To explore whether propyne remains the starting point for C–C bond cleavage on the oxide surfaces, it is useful to examine first the quantitative aspect of the thermodynamics of the side reactions.

It has been demonstrated that the formation of C1 and C2 species in PDH is a consequence of the competition between the C–H and C–C bond cleavage.[68,77] Thus, the reaction energies for the C–H and C–C bond breaking of propylene and five deeply dehydrogenated C3 intermediates at the Ga(o)–O and Pt–O′ sites are calculated and compared in Figure S6. From the figure, one can see that all the reaction energies for the C–C bond breaking of the C3 species are more positive than 1.9 eV, implying the cracking reaction can hardly occur because the energy barriers that must be even more positive cannot be surmounted under the reaction conditions. It is important to note that, despite the high reactivity of single Pt atoms, C–C bond breaking is also inhibited so that a high selectivity can be attained on Pt_1–Ga_2O_3(100) (see Figure S6), which can be explained by the fact that the surface doped with single metal atoms could not provide a sufficiently large ensemble to stabilize the resultant big fragments.[78] In addition, because cracking reactions may be promoted by Lewis acid sites, we have also examined the cracking reactions at the O_3–Ga(o)–OH site. It can be seen in Figure S6 that the reaction energies for the C–C bond breaking of all the C3 species at the O_3–Ga(o)–OH site are more positive than 2.5 eV, implying the cracking reactions can hardly occur under the relevant conditions.

As aforementioned, Ga_2O_3 is difficult to be reduced by H_2, but surface oxygen vacancies may result when it is brought into contact with alkanes.[8] Thus, to reveal the real active site for the cracking reactions, we considered oxygen vacancies that may assist in rupturing C–C bonds. Figure 8a shows the comparison of the reaction energies on the oxygen-deficient surface. It can be seen that the reaction energies for the C–C bond breaking of the C3 species become less positive than those on the pristine surface, and propyne is the sole species that has a cracking energy comparable to that for dehydrogenation. Then, the transition states for the C–H and C–C bond breaking of propyne are located, and the energy profiles are shown in Figure 8b. It can be seen that the energy barriers for the cracking of propyne is 0.50 eV lower than that for the C–H bond cleavage, indicating that propyne prefers cracking to dehydrogenation. The computed charge density difference also supports this idea by showing that the electrons left behind upon oxygen removal would be localized primarily around the two C–Ga(o) bonds while the C–C triple bond is substantially weakened. Hence, propyne should be the starting point for C–C bond breaking in PDH over the Ga_2O_3 catalyst.

Microkinetic analysis

Although the analysis of the energetics and electronic structures can provide a useful first description of the kinetics of the PDH reaction, previous microkinetic analysis and kinetic Monte Carlo simulations carried out on the Pt catalyst suggested that the kinetics obtained in this way may not be entirely accurate in all details,[79-81] especially when the contributions from different active sites need to be considered. Thus, microkinetic analysis was conducted on Pt_1–Ga_2O_3(100) to identify the active sites responsible for the high catalytic efficiency of the single-atom-doped catalyst and hence to formulate the overall reaction mechanism.

The postulated reaction network for PDH is given in Table S4, where "*o*", "*i*", and "*s*" refer to the Ga(o)–O, Ga(o)′–O′, and Pt–O′ sites, respectively. Since H diffusion on the oxide surface is predicted to occur very rapidly, the mean-field approximation is used to solve the microkinetic model. Also, we assume to a first approximation that equilibrium is established between the adsorbed H on the three types of active sites. To mimic the Pt_1–Ga_2O_3(100) surface, 5% of the exposed Ga(o) ions on Ga_2O_3(100) are replaced with Pt ions on account of the low Pt loading (0.1 wt%) used in experiment (The detailed reason can be found in Sec. 13 in the Supporting Information).[18] Accordingly, 10% of the surface Ga(o) ions that are adjacent to the Pt ions exhibit different physiochemical properties from the remaining Ga(o) ions on the surface. Thus, the Pt_1–Ga_2O_3(100) surface comprises 5% Pt–O′ site, 10% Ga(o)′–O′ site, and 85% Ga(o)–O site.

The calculated turnover frequencies (TOFs) on Ga_2O_3(100) and Pt_1–Ga_2O_3(100) at 895 K and 1 bar of C_3H_8 are presented in Figure 9. From the figure, one can see that the TOF for propane consumption is calculated to be 1.78×10^{-4} s^{-1} on the pristine surface that is surrounded entirely by the Ga(o)–O site, which falls within the experimentally reported range for the GaO_x-based catalysts.[1] On the Pt_1–Ga_2O_3(100) surface, the TOF for propane consumption is calculated to be 5.04×10^{-4} s^{-1}, meaning that the reaction would occur nearly 2.8 times faster than that on Ga_2O_3(100), which agrees remarkably good with the experimental observation by Sattler et al.[18] In their work, the conversion of propane at the beginning of the reaction almost doubles after introducing 1000 ppm Pt to the 3 wt % Ga_2O_3/Al_2O_3 catalyst.[18] Very interestingly, it is found that the Pt_1–Ga_2O_3(100) catalyst shows a bifunctional character. As shown in Figure 9, the Pt–O′ site accounts for 68.7% of the TOF for propane consumption; that is, this ion pair plays a major role in C–H bond activation and brings about dehydrogenation. On the other hand, the Ga(o)–O site accounts for 66.0% of the TOF for hydrogen desorption, and is therefore the main active site for H–H bond formation. The remaining Ga(o)′–O′ sites that surround the Pt ions make a negligible contribution to the overall rate of the reaction.

The degrees of rate control are then calculated and listed in Table S5, which show that the first dehydrogenation step with the formation of 2-propyl&H is invariably the rate-determining step for the dominant PDH reaction pathway on both the two surfaces. As discussed in Sec. 3.4.1, the formation of 2-propyl&H is kinetically promoted at the Pt–O′ site. It is therefore not surprising to learn that the TOFs are increased on Pt_1–Ga_2O_3(100). The surface coverages of the intermediates

are summarized in Table S6. It can be seen that, the coverage of free sites approaches unity on the two surfaces and, consequently, the adsorbed species, such as H attached to the Ga and O site, have a minor impact on the PDH kinetics. Given the fact that the PDH reaction follows a mechanism with a slow initial step, the overall reaction rate is determined by the energy barrier for the rate-determining step. Therefore, the lower activation energy for propane activation at the Pt–O site explains the higher catalytic activity than that of the pristine Ga_2O_3 catalyst. This finding provides a beautiful explanation for the experimental observation by Sattler et al.[18] who found that even trace amounts of Pt can dramatically improve the catalytic performance of Ga_2O_3.

CONCLUSIONS

In this work, the kinetics of propane dehydrogenation over Pt_1–Ga_2O_3(100) has been studied by combining DFT calculations and microkinetic analysis. It is found that the Pt-doped Ga_2O_3 catalyst shows a bifunctional character. At the Ga(o)–O site, the Lewis acid-base interaction occurs when a pair of amphoteric species are coadsorbed, which makes it kinetically feasible for two H atoms to be coadsorbed at the Ga(o) and O ion pair and thus has a positive effect on hydrogen recombination. Through energy decomposition and electronic structure analysis, for this first time, the strength of the Lewis acid-base interaction is quantitatively measured and the accompanying electron transfer between the two coadsorbed species through the oxide surface is visualized.

Because the doped Pt has *d* orbitals both occupied and unoccupied near the Fermi level and the surrounding O′ ions are less negatively charged, the Pt-O′ site is more active for the activation of propane than the Ga(o)–O site and the activation energy for the rate-limiting step is lowered by more than 0.2 eV. The Pt doping not only can improve the selectivity of the Ga_2O_3 catalyst by hindering the deep dehydrogenation reactions but also helps to achieve a long-term stability by improving the resistance of Ga_2O_3 to hydrogen reduction.

The cracking reaction can only take place after the oxide surface is brought into contact with carbon-containing species to give rise to surface oxygen vacancies, and propyne is suggested to be the starting point for C–C bond breaking. The presence of propyl at the metal site would accelerate the migration of the detached H atoms along the [010] axis, and the mean-field approximation holds well over the oxide surface.

Microkinetic analysis indicates that the Pt–O′ site accounts for 68.7% of the TOF for propane consumption while the Ga(o)–O site accounts for 66.0% of the TOF for hydrogen desorption. As a consequence, the reaction occurs nearly 2.8 times faster than that on the pristine Ga_2O_3 surface, which provides direct theoretical evidence that Pt may play a significant role in improving the catalytic performance of the Ga_2O_3 catalyst in PDH.

ACKNOWLEDGMENTS

This work is supported by the Natural Science Foundation of China (91645122, 21473053, and U1663221), the National Key Research and Development Program of China (2018YFB0604700), and the Fundamental Research Funds for the Central Universities (222201718003). The computational time provided by the Notur project is highly acknowledged.

REFERENCES

1. Sattler JJ, Ruiz-Martinez J, Santillan-Jimenez E, Weckhuysen BM. Catalytic dehydrogenation of light alkanes on metals and metal oxides. *Chem Rev.* 2014;114(20):10613-10653.
2. Bruijnincx PCA, Weckhuysen BM. Shale Gas Revolution: An Opportunity for the Production of Biobased Chemicals? *Angew Chem, Int Ed.* 2013;52(46):11980-11987.
3. Zhao ZJ, Chiu CC, Gong JL. Molecular understandings on the activation of light hydrocarbons over heterogeneous catalysts. *Chem Sci.* 2015;6(8):4403-4425.
4. Michorczyk P, Ogonowski J. Dehydrogenation of propane to propene over gallium oxide in the presence of CO_2. *Appl Catal A.* 2003;251(2):425-433.
5. Zheng B, Hua WM, Yue YH, Gao Z. Dehydrogenation of propane to propene over different polymorphs of gallium oxide. *J Catal.* 2005;232(1):143-151.
6. Xu BJ, Zheng B, Hua WM, Yue YH, Gao Z. Support effect in dehydrogenation of propane in the presence of CO_2 over supported gallium oxide catalysts. *J Catal.* 2006;239(2):470-477.
7. Liu G, Zhao Z-J, Wu T, Zeng L, Gong J. Nature of the Active Sites of VO_x/Al_2O_3 Catalysts for Propane Dehydrogenation. *ACS Catal.* 2016;6(8):5207-5214.
8. Zhao ZJ, Wu T, Xiong C, et al. Hydroxyl-mediated non-oxidative propane dehydrogenation over VO_x/γ-Al_2O_3 catalysts with improved stability. *Angew Chem, Int Ed.* 2018;57(23):6791-6795.
9. Wu TF, Liu G, Zeng L, et al. Structure and Catalytic Consequence of Mg-Modified VO_x/Al_2O_3 Catalysts for Propane Dehydrogenation. *AlChE J.* 2017;63(11):4911-4919.
10. Otroshchenko T, Sokolov S, Stoyanova M, et al. ZrO_2-Based Alternatives to Conventional Propane Dehydrogenation Catalysts: Active Sites, Design, and Performance. *Angew Chem, Int Ed.* 2015;54(52):15880-15883.
11. Otroshchenko T, Kondratenko VA, Rodemerck U, Linke D, Kondratenko EV. ZrO_2-based unconventional catalysts for non-oxidative propane dehydrogenation: Factors determining catalytic activity. *J Catal.* 2017;348:282-290.
12. Zhang YY, Zhao Y, Otroshchenko T, et al. Control of coordinatively unsaturated Zr sites in ZrO_2 for efficient C-H bond activation. *Nat Commun.* 2018;9:10.
13. Xiong HF, Lin S, Goetze J, et al. Thermally Stable and Regenerable Platinum-Tin Clusters for Propane Dehydrogenation Prepared by Atom Trapping on Ceria. *Angew Chem, Int Ed.* 2017;56(31):8986-8991.
14. Wang T, Jiang F, Liu G, Zeng L, Zhao ZJ, Gong JL. Effects of Ga doping on Pt/CeO_2-Al_2O_3 catalysts for propane dehydrogenation. *AlChE J.* 2016;62(12):4365-4376.

15. Liu G, Zeng L, Zhao ZJ, Tian H, Wu TF, Gong JL. Platinum-modified ZnO/Al_2O_3 for propane dehydrogenation: Minimized platinum usage and improved catalytic stability. *ACS Catal.* 2016;6(4):2158-2162.

16. Jiang F, Zeng L, Li S, Liu G, Wang S, Gong J. Propane Dehydrogenation over $Pt/TiO_2–Al_2O_3$ Catalysts. *ACS Catal.* 2015;5(1):438-447.

17. Dixit M, Kostetskyy P, Mpourmpakis G. Structure–Activity Relationships in Alkane Dehydrogenation on γ-Al_2O_3: Site-Dependent Reactions. *ACS Catal.* 2018:11570-11578.

18. Sattler JJ, Gonzalez-Jimenez ID, Luo L, et al. Platinum-promoted Ga/Al_2O_3 as highly active, selective, and stable catalyst for the dehydrogenation of propane. *Angew Chem, Int Ed.* 2014;53(35):9251-9256.

19. Im J, Choi M. Physicochemical Stabilization of Pt against Sintering for a Dehydrogenation Catalyst with High Activity, Selectivity, and Durability. *ACS Catal.* 2016;6(5):2819-2826.

20. Liu Y, Li ZH, Lu J, Fan KN. Periodic density functional theory study of propane dehydrogenation over perfect Ga_2O_3(100) surface. *J Phys Chem C.* 2008;112(51):20382-20392.

21. Qiao B, Wang A, Yang X, et al. Single-atom catalysis of CO oxidation using Pt_1/FeO_x. *Nat Chem.* 2011;3(8):634-641.

22. Moses-DeBusk M, Yoon M, Allard LF, et al. CO oxidation on supported single Pt atoms: experimental and ab initio density functional studies of CO interaction with Pt atom on θ-Al_2O_3(010) surface. *J Am Chem Soc.* 2013;135(34):12634-12645.

23. Gu X-K, Qiao B, Huang C-Q, et al. Supported single Pt_1/Au_1 atoms for methanol steam reforming. *ACS Catal.* 2014;4(11):3886-3890.

24. Nie L, Mei D, Xiong H, et al. Activation of surface lattice oxygen in single-atom Pt/CeO_2 for low-temperature CO oxidation. *Science.* 2017;358(6369):1419-1423.

25. Cheng MJ, Clark EL, Pham HH, Bell AT, Head-Gordon M. Quantum Mechanical Screening of Single-Atom Bimetallic Alloys for the Selective Reduction of CO_2 to C_1 Hydrocarbons. *ACS Catal.* 2016;6(11):7769-7777.

26. Darby MT, Reocreux R, Sykes ECH, Michaelides A, Stamatakis M. Elucidating the Stability and Reactivity of Surface Intermediates on Single-Atom Alloy Catalysts. *ACS Catal.* 2018;8(6):5038-5050.

27. Greiner MT, Jones TE, Beeg S, et al. Free-atom-like d states in single-atom alloy catalysts. *Nat Chem.* 2018.

28. Marcinkowski MD, Darby MT, Liu J, et al. Pt/Cu single-atom alloys as coke-resistant catalysts for efficient C-H activation. *Nat Chem.* 2018;10(3):325-332.

29. Xu GL, Wang R, Yang F, Ma DW, Yang ZX, Lu ZS. CO oxidation on single Pd atom embedded defect-graphene via a new termolecular Eley-Rideal mechanism. *Carbon.* 2017;118:35-42.

30. Feng YX, Zhou LS, Wan Q, Lin S, Guo H. Selective hydrogenation of 1,3-butadiene catalyzed by a single Pd atom anchored on graphene: the importance of dynamics. *Chem Sci.* 2018;9(27):5890-5896.

31. Yan H, Zhao X, Guo N, et al. Atomic engineering of high-density isolated Co atoms on graphene with proximal-atom controlled reaction selectivity. *Nat Commun.* 2018;9(1):3197.

32. Sun G, Zhao ZJ, Mu R, et al. Breaking the scaling relationship via thermally stable Pt/Cu single atom alloys for catalytic dehydrogenation. *Nat Commun.* 2018;9(1):4454.

33. Wang AQ, Li J, Zhang T. Heterogeneous single-atom catalysis. *Nat Rev Chem.* 2018;2(6):65-81.

34. Metiu H, Chretien S, Hu ZP, Li B, Sun XY. Chemistry of Lewis Acid-Base Pairs on Oxide Surfaces. *J Phys Chem C.* 2012;116(19):10439-10450.

35. Li B, Metiu H. Dissociation of Methane on La_2O_3 Surfaces Doped with Cu, Mg, or Zn. *J Phys Chem C.* 2011;115(37):18239-18246.

36. Li B, Metiu H. Does Halogen Adsorption Activate the Oxygen Atom on an Oxide Surface? I. A Study of Br_2 and HBr Adsorption on La_2O_3 and La_2O_3 Doped with Mg or Zr. *J Phys Chem C.* 2012;116(6):4137-4148.

37. Xin Y, Zhang NN, Li Q, et al. Active Site Identification and Modification of Electronic States by Atomic-Scale Doping To Enhance Oxide Catalyst Innovation. *ACS Catal.* 2018;8(2):1399-1404.

38. Riley C, Zhou S, Kunwar D, et al. Design of Effective Catalysts for Selective Alkyne Hydrogenation by Doping of Ceria with a Single-Atom Promotor. *J Am Chem Soc.* 2018;140(40):12964-12973.

39. Liu PX, Zhao Y, Qin RX, et al. A vicinal effect for promoting catalysis of Pd_1/TiO_2: supports of atomically dispersed catalysts play more roles than simply serving as ligands. *Sci Bull.* 2018;63(11):675-682.

40. Kresse G, Hafner J. Ab initio molecular dynamics for liquid metals. *Phys Rev B.* 1993;47(1):558-561.

41. Kresse G, Furthmüller J. Efficiency of ab-initio total energy calculations for metals and semiconductors using a plane-wave basis set. *Comp Mater Sci.* 1996;6(1):15-50.

42. Kresse G, Furthmüller J. Efficient iterative schemes for ab initio total-energy calculations using a plane-wave basis set. *Phys Rev B.* 1996;54(16):11169-11186.

43. Wellendorff J, Lundgaard KT, Mogelhoj A, et al. Density functionals for surface science: Exchange-correlation model development with Bayesian error estimation. *Phys Rev B.* 2012;85(23):23.

44. Henkelman G, Jonsson H. A dimer method for finding saddle points on high dimensional potential surfaces using only first derivatives. *J Chem Phys.* 1999;111(15):7010-7022.

45. Henkelman G, Uberuaga BP, Jonsson H. A climbing image nudged elastic band method for finding saddle points and minimum energy paths. *J Chem Phys.* 2000;113(22):9901-9904.

46. Henkelman G, Jonsson H. Improved tangent estimate in the nudged elastic band method for finding minimum energy paths and saddle points. *J Chem Phys.* 2000;113(22):9978-9985.

47. Kohn J, Katz G, Broder J. Characterization of β-Ga_2O_3 and its Alumina Isomorph, θ-Al_2O_3. *Am Mineral.* 1957;42(5-6):398-407.

48. Geller S. Crystal Structure of β-Ga_2O_3. *J Chem Phys.* 1960;33(3):676-684.

49. Bermudez VM. The structure of low-index surfaces of β-Ga_2O_3. *Chem Phys.* 2006;323(2-3):193-203.

50. Guo W, Guo Y, Dong H, Zhou X. Tailoring the electronic structure of β-Ga_2O_3 by non-metal doping from hybrid density functional theory calculations. *Phys Chem Chem Phys.* 2015;17(8):5817-5825.

51. Kyrtsos A, Matsubara M, Bellotti E. Migration mechanisms and diffusion barriers of vacancies in Ga_2O_3. *Phys Rev B.* 2017;95(24):9.

52. Calatayud M, Collins SE, Baltanas MA, Bonivardi AL. Stability of formate species on β-Ga_2O_3. *Phys Chem Chem Phys.* 2009;11(9):1397-1405.

53. Pan YX, Mei DH, Liu CJ, Ge QF. Hydrogen Adsorption on Ga_2O_3 Surface: A Combined Experimental and Computational Study. *J Phys Chem C.* 2011;115(20):10140-10146.

54. Ma YQ, Zhao X, Niu MM, et al. Monoclinic Ga_2O_3(100) surface as a robust photocatalyst for water-splitting. *RSC Adv.* 2017;7(7):4124-4134.

55. Liu JY. Catalysis by Supported Single Metal Atoms. *ACS Catal.* 2017;7(1):34-59.

56. Wan J, Chen W, Jia C, et al. Defect Effects on TiO_2 Nanosheets: Stabilizing Single Atomic Site Au and Promoting Catalytic Properties. *Adv Mater.* 2018;30(11).

57. Ma XL, Liu JC, Xiao H, Li J. Surface Single-Cluster Catalyst for N_2-to-NH_3 Thermal Conversion. *J Am Chem Soc.* 2018;140(1):46-49.

58. Han ZK, Gao Y. Water Adsorption and Dissociation on Ceria-Supported Single-Atom Catalysts: A First-Principles DFT+U Investigation. *Chemistry.* 2016;22(6):2092-2099.

59. Xu Y, Chen JN, Yuan XL, et al. Sintering-resistant Pt on Ga_2O_3 rods for propane dehydrogenation: The morphology matters. *Ind Eng Chem Res.* 2018;57(39):13087-13093.

60. Medford AJ, Shi C, Hoffmann MJ, et al. CatMAP: A Software Package for Descriptor-Based Microkinetic Mapping of Catalytic Trends. *Catal Lett.* 2015;145(3):794-807.

61. Cortright RD, Dumesic JA. Kinetics of heterogeneous catalytic reactions: Analysis of reaction schemes. *Adv Catal.* 2001;46:161-264.

62. Campbell CT. The degree of rate control: A powerful tool for catalysis research. *ACS Catal.* 2017;7(4):2770-2779.

63. Stegelmann C, Andreasen A, Campbell CT. Degree of rate control: how much the energies of intermediates and transition states control rates. *J Am Chem Soc.* 2009;131(23):8077-8082.

64. Kostestkyy P, Yu J, Gorte RJ, Mpourmpakis G. Structure–activity relationships on metal-oxides: alcohol dehydration. *Catal Sci Technol.* 2014;4(11):3861-3869.

65. McFarland EW, Metiu H. Catalysis by doped oxides. *Chem Rev.* 2013;113(6):4391-4427.

66. Lang R, Xi W, Liu JC, et al. Non defect-stabilized thermally stable single-atom catalyst. *Nat Commun.* 2019;10.

67. Chang QY, Yin Q, Ma F, et al. Tuning adsorption and catalytic properties of α-Cr_2O_3 and ZnO in propane dehydrogenation by creating oxygen vacancy and doping single Pt atom: A comparative first-principles study. *Ind Eng Chem Res.* 2019;58(24):10199-10209.

68. Yang ML, Zhu YA, Fan C, Sui ZJ, Chen D, Zhou XG. DFT study of propane dehydrogenation on Pt catalyst: effects of step sites. *Phys Chem Chem Phys.* 2011;13(8):3257-3267.

69. Yang ML, Zhu YA, Zhou XG, Sui ZJ, Chen D. First-principles calculations of propane dehydrogenation over PtSn catalysts. *ACS Catal.* 2012;2(6):1247-1258.

70. Yang M-L, Zhu Y-A, Fan C, Sui Z-J, Chen D, Zhou X-G. Density functional study of the chemisorption of C_1, C_2 and C_3 intermediates in propane dissociation on Pt(111). *J Mol Catal A: Chem.* 2010;321(1-2):42-49.
71. Kazansky VB, Subbotina IR, Pronin AA, Schlogl R, Jentoft FC. Unusual infrared spectrum of ethane adsorbed by gallium oxide. *J Phys Chem B.* 2006;110(15):7975-7978.
72. Gabrienko AA, Arzumanov SS, Toktarev AV, Stepanov AG. Metal-alkyl species are formed on interaction of small alkanes with gallium oxide: Evidence from solid-state NMR. *Chem Phys Lett.* 2010;496(1-3):148-151.
73. Bligaard T, Norskov JK, Dahl S, Matthiesen J, Christensen CH, Sehested J. The Bronsted-Evans-Polanyi relation and the volcano curve in heterogeneous catalysis. *J Catal.* 2004;224(1):206-217.
74. Nykänen L, Honkala K. Selectivity in Propene Dehydrogenation on Pt and Pt3Sn Surfaces from First Principles. *ACS Catal.* 2013;3(12):3026-3030.
75. Collins S, Baltanas M, Garciafierro J, Bonivardi A. Gallium–Hydrogen Bond Formation on Gallium and Gallium–Palladium Silica-Supported Catalysts. *J Catal.* 2002;211(1):252-264.
76. Saito M, Watanabe S, Takahara I, Inaba M, Murata K. Dehydrogenation of propane over a silica-supported gallium oxide catalyst. *Catal Lett.* 2003;89(3-4):213-217.
77. Yang M-L, Fan C, Zhu Y-A, Sui Z-J, Zhou X-G, Chen D. Selective Oxidation of Hydrogen in the Presence of Propylene over Pt-Based Core–Shell Nanocatalysts. *J Phys Chem C.* 2015;119(37):21386-21394.
78. Wang HF, Wang D, Liu XH, Guo YL, Lu GZ, Hu PJ. Unexpected C-C Bond Cleavage Mechanism in Ethylene Combustion at Low Temperature: Origin and Implications. *ACS Catal.* 2016;6(8):5393-5398.
79. Saerens S, Sabbe MK, Galvita VV, Redekop EA, Reyniers MF, Marin GB. The Positive Role of Hydrogen on the Dehydrogenation of Propane on Pt(111). *ACS Catal.* 2017;7(11):7495-7508.
80. Lian Z, Ali S, Liu TF, Si CW, Li B, Su DS. Revealing the Janus character of the coke precursor in the propane direct dehydrogenation on Pt catalysts from a kMC simulation. *ACS Catal.* 2018;8(5):4694-4704.
81. Zha SJ, Sun GD, Wu TF, Zhao JB, Zhao ZJ, Gong JL. Identification of Pt-based catalysts for propane dehydrogenation via a probability analysis. *Chem Sci.* 2018;9(16):3925-3931.

SUPPORTING INFORMATION

Additional supporting information may be found online in the Supporting Information section at the end of this article.

List of Figure Captions

Figure 1. (a) Side and top views of the slab model of Pt_1–Ga_2O_3(100), charge density difference for the adsorption of (b) Ga(o) and (c) Pt in the metal vacancy, density of states projected onto the O 2*p* and metal valence shell at the (d) Ga(o)–O and (e) Pt–O′–Ga(o)′ sites. Charge accumulation and depletion are colored yellow and cyan, respectively, with the isosurface value being 0.04 e/Å^3.

Figure 2. Decomposition of adsorption energies of propylene on Pt_1–Ga_2O_3(100).

Figure 3. Computed charge density difference for H adsorption at the O site with another H atom pre-adsorbed at the adjacent (a) Ga(o), (b) Ga(o)′, and (c) Pt site. Charge accumulation and depletion are colored yellow and cyan, respectively, with the isosurface value being 0.04 e/Å^3.

Figure 4. Energy profiles for the main reaction of PDH via the formation of (a) 1-propyl and (b) 2-propyl on Pt_1–Ga_2O_3(100) as well as the geometries of the transition states for the elementary steps involved. All the potential energies are referenced to the sum of the total energies of gas-phase propane and the bare oxide surface.

Figure 5. Illustration of H migration elementary steps on the surfaces around the Ga(o) and Pt ions (a, b) with and (c, d) without 2-propyl adsorbed in the vicinity and (e) calculated H migration barriers.

Figure 6. Energy profiles and geometries of the transition states for H_2 desorption and H_2O formation on Pt_1–Ga_2O_3(100). All the potential energies are referenced to the sum of the total energies of gas-phase H_2 and the bare oxide surface. Charge accumulation and depletion are colored yellow and cyan, respectively, with the isosurface value being 0.04 e/Å^3.

Figure 7. Energy profiles for the deep dehydrogenation of propylene via the formation of (a) 1-propenyl and (b) 2-propenyl on Pt_1-Ga_2O_3(100) as well as the geometries of the transition states for the elementary steps involved. All the potential energies are referenced to the sum of total energies of gas-phase propane and the bare oxide surface.

Figure 8. (a) Comparison of the reaction energies for C-H and C-C bond breaking of propylene and five deeply dehydrogenated C3 intermediates on the oxygen-deficient Ga_2O_3(100) surface and (b) potential energy diagrams for propyne dehydrogenation and cracking as well as the geometries of the initial and transition states. All the potential energies are referenced to the sum of the total energies of gas-phase propane and the defective surface. Charge accumulation and depletion are colored yellow and cyan, respectively, with the isosurface value being 0.04 e/Å^3.

Figure 9. TOFs on Ga_2O_3(100) and Pt_1–Ga_2O_3(100) at 895K and 1 bar of C_3H_8.

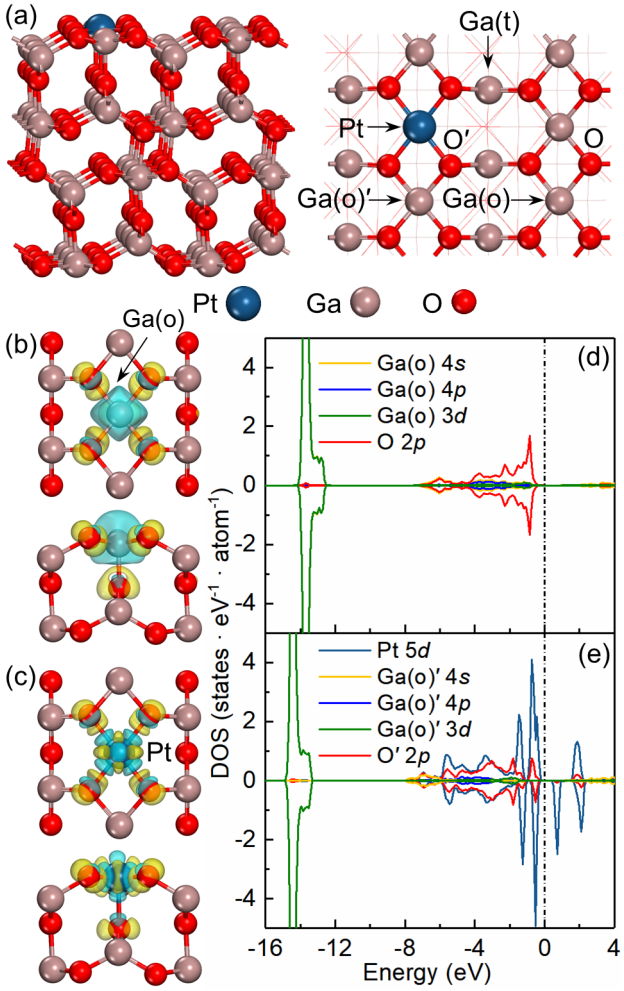

Figure 1. (a) Side and top views of the slab model of Pt_1–Ga_2O_3(100), charge density difference for the adsorption of (b) Ga(o) and (c) Pt in the metal vacancy, density of states projected onto the O 2*p* and metal valence shell at the (d) Ga(o)–O and (e) Pt–O′–Ga(o)′ sites. Charge accumulation and depletion are colored yellow and cyan, respectively, with the isosurface value being 0.04 e/Å^3.

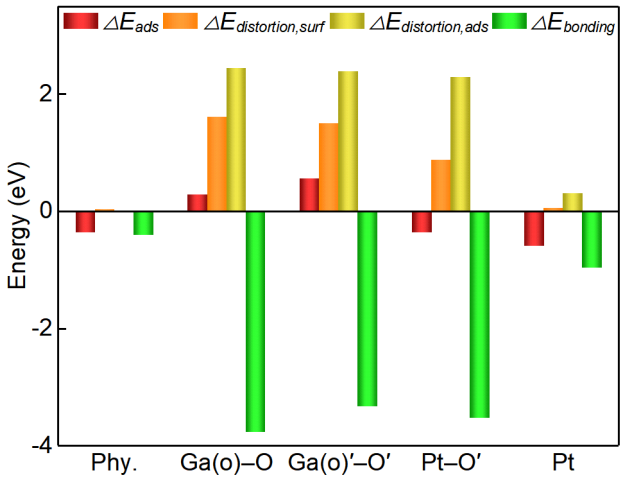

Figure 2. Decomposition of adsorption energies of propylene on Pt_1–Ga_2O_3(100).

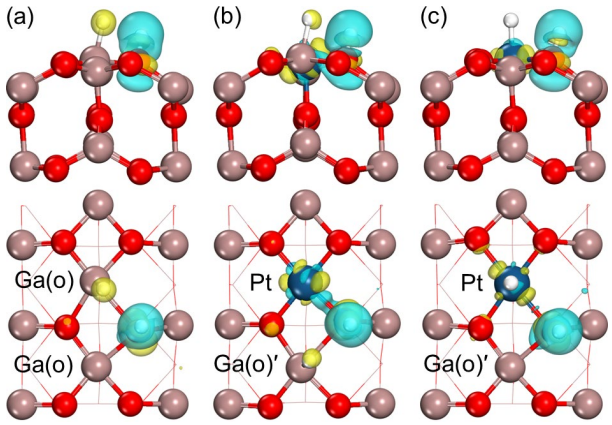

Figure 3. Computed charge density difference for H adsorption at the O site with another H atom pre-adsorbed at the adjacent (a) Ga(o), (b) Ga(o)′, and (c) Pt site. Charge accumulation and depletion are colored yellow and cyan, respectively, with the isosurface value being 0.04 e/Å^3.

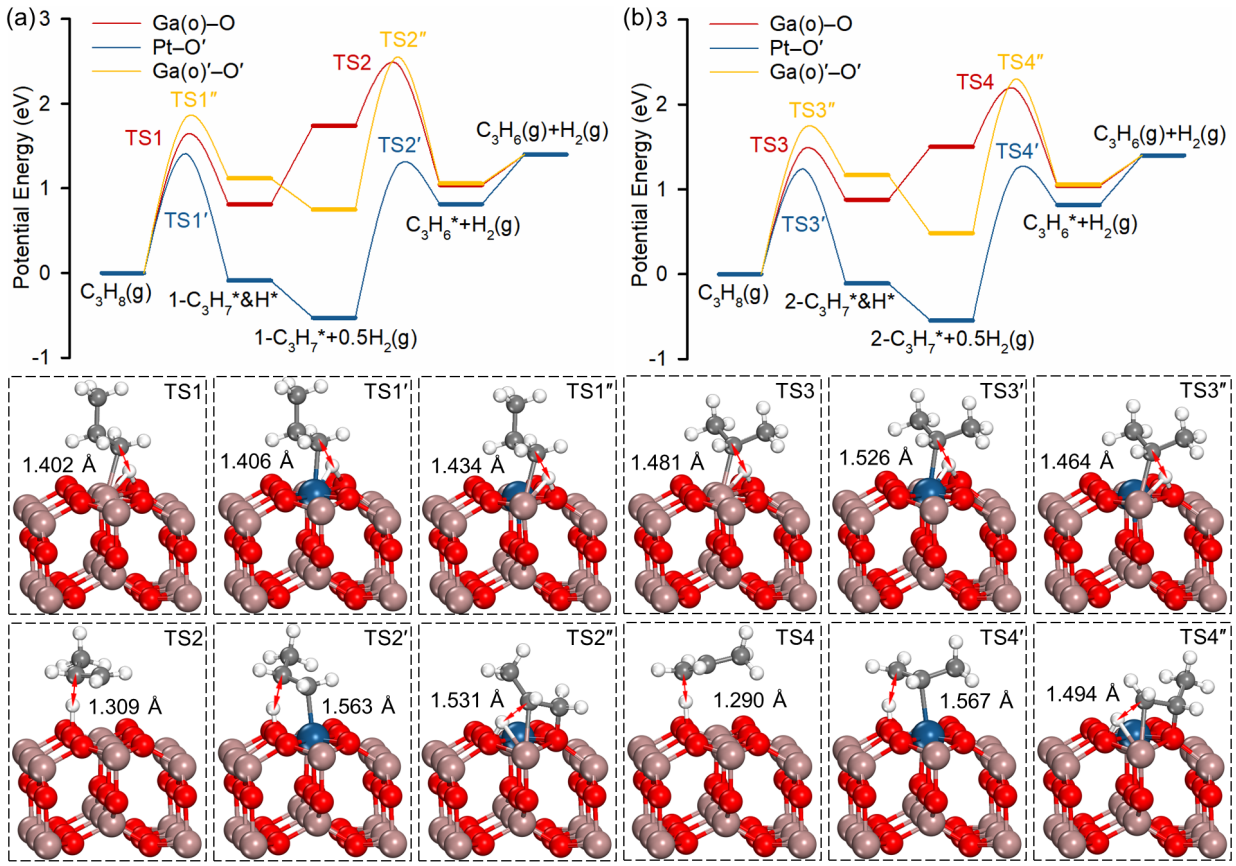

Figure 4. Energy profiles for the main reaction of PDH via the formation of (a) 1-propyl and (b) 2-propyl on Pt_1–Ga_2O_3(100) as well as the geometries of the transition states for the elementary steps involved. All the potential energies are referenced to the sum of the total energies of gas-phase propane and the bare oxide surface.

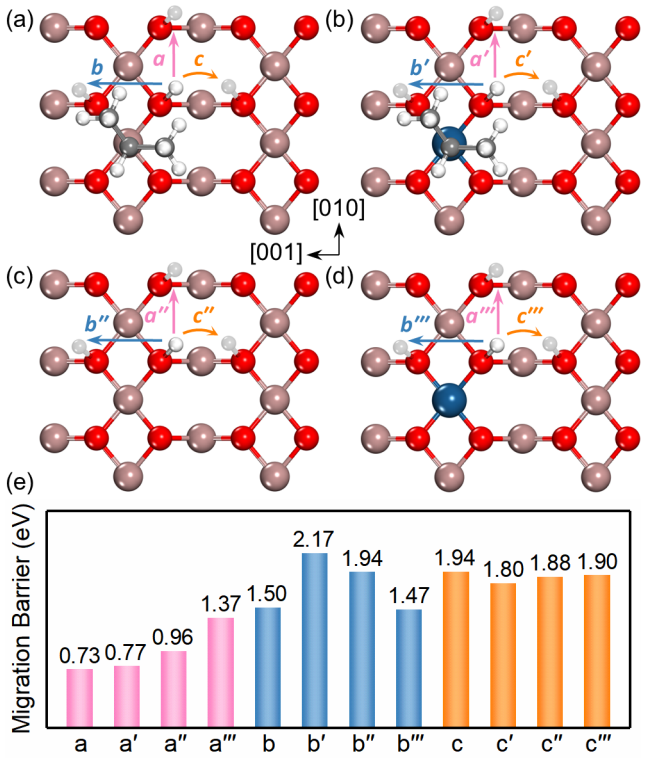

Figure 5. Illustration of H migration elementary steps on the surfaces around the Ga(o) and Pt ions (a, b) with and (c, d) without 2-propyl adsorbed in the vicinity and (e) calculated H migration barriers.

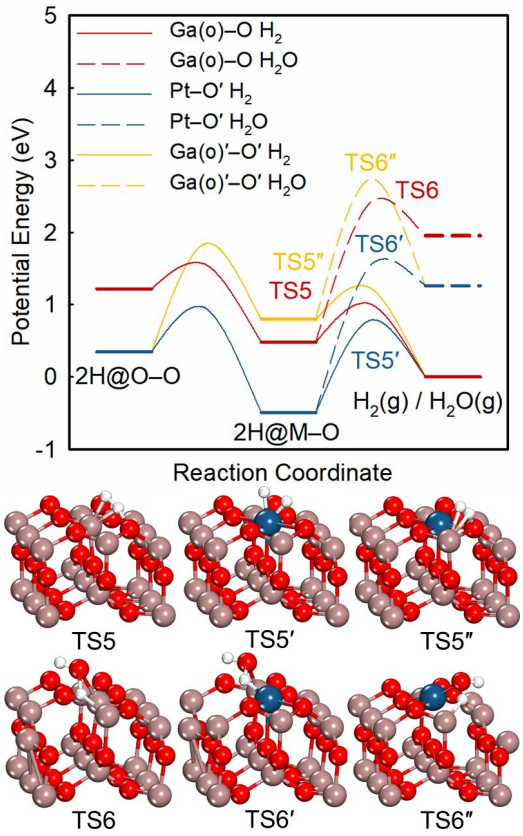

Figure 6. Energy profiles and geometries of the transition states for H_2 desorption and H_2O formation on Pt_1–Ga_2O_3(100). All the potential energies are referenced to the sum of the total energies of gas-phase H_2 and the bare oxide surface. Charge accumulation and depletion are colored yellow and cyan, respectively, with the isosurface value being 0.04 e/Å^3.

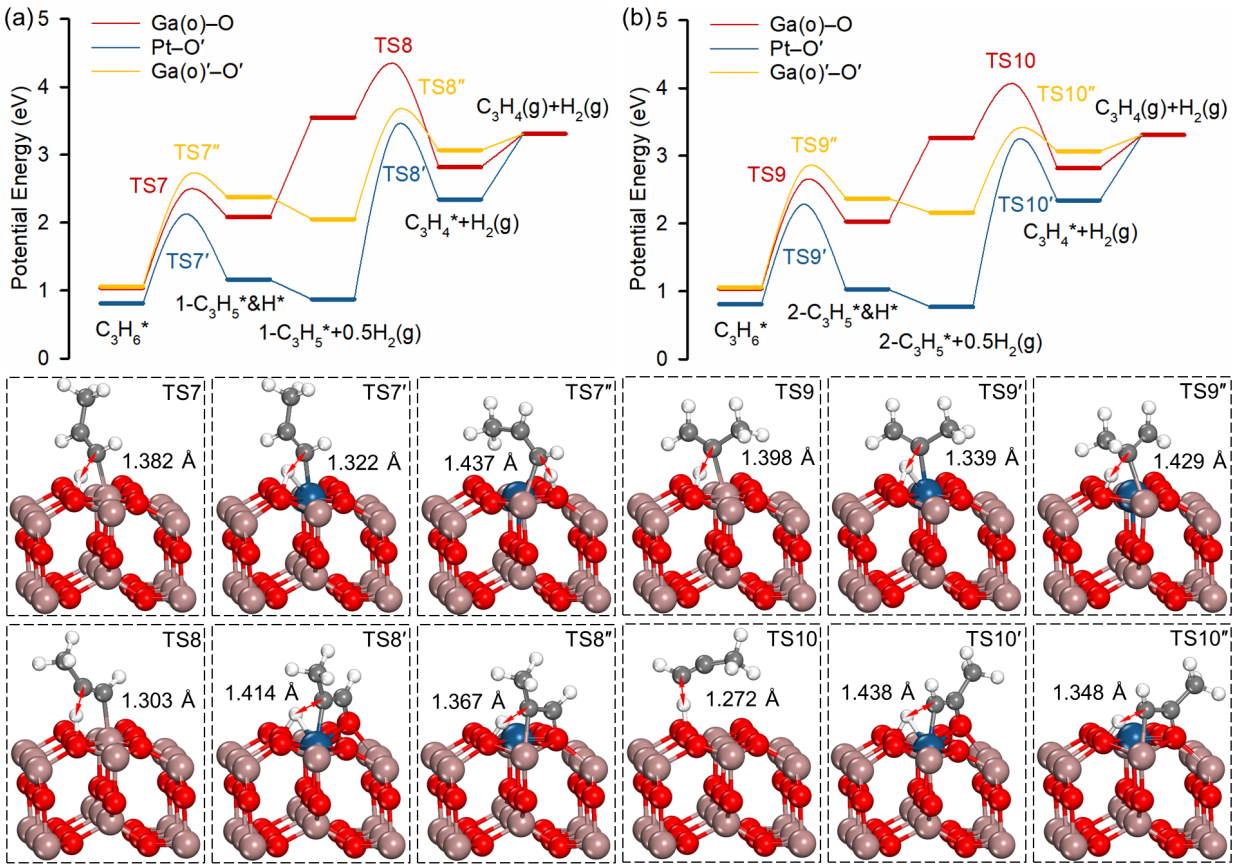

Figure 7. Energy profiles for the deep dehydrogenation of propylene via the formation of (a) 1-propenyl and (b) 2-propenyl on Pt_1-Ga_2O_3(100) as well as the geometries of the transition states for the elementary steps involved. All the potential energies are referenced to the sum of total energies of gas-phase propane and the bare oxide surface.

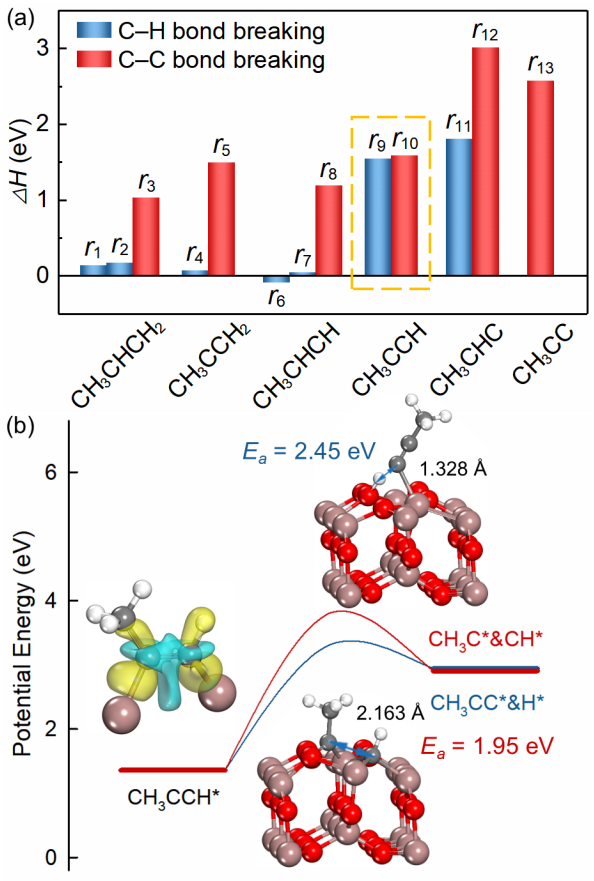

Figure 8. (a) Comparison of the reaction energies for C-H and C-C bond breaking of propylene and five deeply dehydrogenated C3 intermediates on the oxygen-deficient $Ga_2O_3(100)$ surface and (b) potential energy diagrams for propyne dehydrogenation and cracking as well as the geometries of the initial and transition states. All the potential energies are referenced to the sum of the total energies of gas-phase propane and the defective surface. Charge accumulation and depletion are colored yellow and cyan, respectively, with the isosurface value being 0.04 e/Å^3.

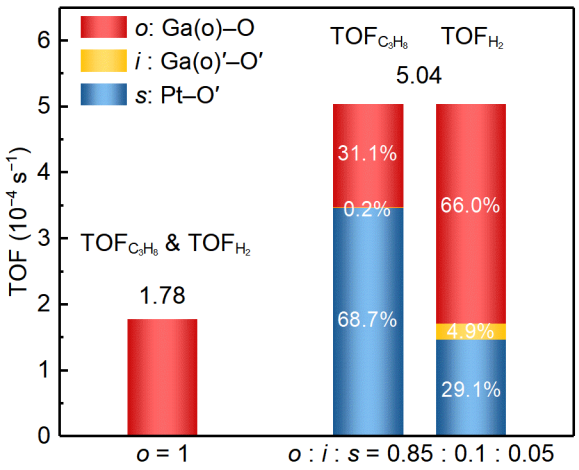

Figure 9. TOFs on $Ga_2O_3(100)$ and Pt_1–$Ga_2O_3(100)$ at 895K and 1 bar of C_3H_8.

Table 1. Calculated adsorption energies and effective Bader charge on adsorbed species.

Species	Site	ΔE_{ads} /eV	Effective Bader charge on adsorbed species/|e|
Propane	Physisorbed	−0.25	-
H_2	Physisorbed	−0.07	-
Propylene	Physisorbed	−0.35	-
	Ga(o)–O	0.29	-
	Ga(o)′–O′	0.56	-
	Pt–O′	−0.36	-
	Pt	−0.59	-
H	O	−2.17	0.54+
	Ga(o)	−0.16	0.20−
	O′	−2.59	0.56+
	Ga(o)′	−0.37	0.26–
	Pt	−3.27	0.03−
1-propyl	Physisorbed	−0.40	-
	O	−1.03	0.53+
	O′	−1.39	0.54+
	Pt	−2.66	0.06+
2-propyl	Physisorbed	−0.46	-
	O	−0.94	0.54+
	O′	−1.48	0.54+
	Pt	−2.54	0.08+

Table 2. Calculated Lewis acid-base interaction, adsorption energy difference, and effective Bader charge carried by adsorbed species on Pt_1–Ga_2O_3(100).

Coadsorbed species	Site	$\Delta E_{int,acid-base}$ /eV	$\Delta E_{coads} - \Delta E_{ads,acid} - \Delta E_{ads,base}$ /eV	Effective Bader charge on adsorbed species/|e|
H&H	Ga(o)–O	−1.77	−2.03	0.36− & 0.56+
	Ga(o)′–O′	−1.61	−1.08	0.37− & 0.57+
	Pt–O′	0.09	0.53	0.03− & 0.55+
1-propyl&H	Ga(o)–O	−1.38	−1.18	0.32− & 0.55+
	Ga(o)′–O′	−1.00	−0.48	0.33– & 0.56+
	Pt–O′	0.24	0.60	0.01– & 0.55+
2-propyl&H	Ga(o)–O	−1.33	−0.88	0.30– & 0.54+
	Ga(o)′–O′	−1.09	−0.19	0.31– & 0.56+
	Pt–O′	0.32	0.63	0.02+ & 0.55+